

Abstract

Using a geometric eddy identification method, cyclonic and anticyclonic eddies from submesoscale to mesoscale in the South Indian Ocean (SIO) have been statistically investigated based on 2082 surface drifters from 1979 to 2013. 19252 eddies are identified with 60 % anticyclonic eddies. For the submesoscale eddies (radius $r < 10$ km), the ratio of cyclonic eddies (3183) to anticyclonic eddies (7182) is 1 to 2. In contrast, number of anticyclonic and cyclonic eddies with radius $r \geq 10$ km is almost equal. Mesoscale and submesoscale eddies show different spatial distribution. Eddies with radius $r \geq 100$ km mainly appear in a band along 25° S, in Mozambique Channel, and Agulhas Current, characterized by large eddy kinetic energy. The submesoscale anticyclonic eddies are densely distributed in the subtropical basin in the central SIO. The number of mesoscale eddies shows statistically significant seasonal variability, reaching a maximum in October and then minimum in February.

1 Introduction

The South Indian Ocean (SIO) has unique current systems. A schematic general circulation diagram is shown in Fig. 1. The South Equatorial Current (SEC) in the SIO is in a large part supplied by the Indonesian Throughflow (ITF). The SEC splits into the Northeast Madagascar Current (NEMC) and Southeast Madagascar Current (SEMC) when it reaches the east coast of Madagascar near 17° S (Schott et al., 2001, 2009). The NEMC flows around the north tip of Madagascar at Cape Amber to the coast of Tanzania at about 12° S, and splits into northward and southward flows. The northward branch of NEMC feeds into the East African Coast Current (EACC), and the southward branch joins the Mozambique Channel throughflow with anticyclonic eddies (De Ruijter et al., 2002; Schouten et al., 2003; Ridderinkhof et al., 2010). The SEMC joins the Agulhas Current after passing south of Madagascar, featured with plentiful eddies and dipoles (De Ruijter et al., 2004; Quartly et al., 2006). The Agulhas Current carries

OSD

11, 2879–2905, 2014

Eddy characteristics in the SIO as inferred from surface drifter

Shaojun Zheng et al.

Title Page

Abstract

Introduction

Conclusions

References

Tables

Figures



Back

Close

Full Screen / Esc

Printer-friendly Version

Interactive Discussion



warm and saline water from the Indian Ocean to the Atlantic Ocean through Agulhas Leakage (Gordon et al., 1992; Donners et al., 2004). The Agulhas retroflexion reenters the SIO as a broad northeastward flow and extends to the west coast of Australia (Schott et al., 2009).

Mesoscale eddies are an important ocean dynamic phenomenon, and provide important material and dynamical fluxes for the equilibrium balances of the general circulation and climate (McWilliams, 2013). Mesoscale eddies can cause heat and salt transports (Qiu and Chen, 2005; Volkov et al., 2008; Dong et al., 2014), and eddy-induced zonal mass transport is comparable in magnitude with that of large scale circulation (Zhang et al., 2014). Mesoscale eddies modulate the nutrient flux into euphotic zone through vertical and horizontal transport (Falkowski et al., 1991; Aristegui et al., 1997; Crawford et al., 2005). Submesoscale eddies also play a key role in biogeochemical budgets through intense upwelling of nutrients, subduction of plankton and horizontal stirring (Ledwell et al., 1993; Abraham, 1998; Abraham et al., 2000; Lévy et al., 2001; Lévy and Klein, 2004). Mesoscale eddies in the SIO have been studied using satellite data (e.g. Palastanga et al., 2006; Chelton et al., 2011), ocean modeling (e.g. Backeberg et al., 2008) and in-situ observations (e.g. de Ruijter et al., 2004; Ridderinkhof et al., 2010). In the southeast Indian Ocean (IO), altimetry measurements showed that anticyclonic eddies propagate westward and equatorward, and cyclonic eddies propagate poleward (Morrow et al., 2004). The eddy kinetic energy (EKE) shows a seasonal cycle with the maximum in summer and the minimum in winter (Jia et al., 2011). In austral spring, the enhanced flux forcing of combined meridional Ekman and geostrophic convergence strengthens the upper-ocean meridional temperature gradient, and intensifies the modulation in the vertical velocity shear. The modulation in the vertical velocity shear changes the intensity of baroclinic instability associated with the surface-intensified South Indian Countercurrent (SICC) and underlying SEC system, leading to the seasonal variations of EKE. In Mozambique Channel, satellite SeaWiFs ocean color snapshots showed that large anticyclonic rings intermittently propagated poleward along the western edge of the channel (Quarty and Srokosz, 2004). Analysis

Eddy characteristics in the SIO as inferred from surface drifter

Shaojun Zheng et al.

[Title Page](#)[Abstract](#)[Introduction](#)[Conclusions](#)[References](#)[Tables](#)[Figures](#)[Back](#)[Close](#)[Full Screen / Esc](#)[Printer-friendly Version](#)[Interactive Discussion](#)

of Satellite Oceanographic data (AVISO). EKE are calculated by geostrophic velocity anomalies (Pujol and Larnicol, 2005; Jia et al., 2011) as follows:

$EKE = \frac{1}{2} (U_g'^2 + V_g'^2)$, $U_g' = -\frac{g}{f} \frac{\Delta\eta'}{\Delta y}$ and $V_g' = \frac{g}{f} \frac{\Delta\eta'}{\Delta x}$, where U_g' and V_g' are the geostrophic velocity anomalies, $\Delta\eta'$ is the SLA.

3 Eddy characteristics and statistics in the SIO

3.1 Number and radius

On the basis of the surface satellite-tracked drifter data, a total of 57 228 loops were detected in the SIO. Among them 22 773 are cyclonic loops and 34 455 are anticyclonic loops. After clustering the loops, total 19 252 eddies are detected with 7657 cyclonic eddies (clockwise) and 11 595 anticyclonic eddies (counter-clockwise). The number of anticyclonic eddies account for 60 % of eddies. Figure 6 shows the histogram of eddy radius with bin width of 5 km, in which blue (red) bars depict cyclonic (anticyclonic) eddies. Submesoscale eddies (radius $r < 10$ km) are identified successfully, and its number is 10 365 accounting for 54 % of total eddies. In term of submesoscale eddies, the ratio of cyclonic eddies to anticyclonic eddies is 1 to 2. With submesoscale eddies excluded, the mean radius are 39, 37, and 41 km for all, cyclonic, and anticyclonic eddies, respectively. As documented by Chaigneau and Pizarro (2005), if drifters are on average statistically evenly distributed along the eddy radius R , the probability density $p(r, \theta)$ of finding the drifter at a radius r and direction θ relative to the eddy center is constant. The formulate is as follows: $p(r, \theta) = \frac{1}{\int_0^R \int_0^{2\pi} r dr d\theta} = \frac{1}{\pi R^2}$. The mean distance $\overline{R_1}$,

or expectation $E(r) = \int_0^R \int_0^{2\pi} r^2 p(r, \theta) dr d\theta$ of drifter from the eddy center is then given

by $\overline{R_1} = 2R/3$. The mean eddy diameter is 38 km in the SIO, implying a characteristic eddy diameter of 57 km. This order of magnitude is consistent with mean Rossby

Eddy characteristics in the SIO as inferred from surface drifter

Shaojun Zheng et al.

Title Page

Abstract

Introduction

Conclusions

References

Tables

Figures



Back

Close

Full Screen / Esc

Printer-friendly Version

Interactive Discussion



Eddy characteristics in the SIO as inferred from surface drifter

Shaojun Zheng et al.

Title Page

Abstract

Introduction

Conclusions

References

Tables

Figures



Back

Close

Full Screen / Esc

Printer-friendly Version

Interactive Discussion



of Madagascar. In the Mozambique Channel, the shape of large eddies is restrained by coastline in northeast-southwest direction. Middle eddies have similar spatial distribution to that of large eddies, but occur in a wider area. Middle eddies number is about 2 times the number of large eddies (Fig. 9b). Unlike other kind eddies, the number of small cyclonic eddies is greater than small anticyclonic eddies (Fig. 9c). The small eddies are in the region range from 20 to 44° S, and the distribution of cyclonic eddies appear northeast-southwest direction in the west of Australia. Here the distribution of cyclonic eddies is consistent with poleward propagation in the eastern boundary, which can be explained by theories for vortex propagation on β plane (Morrow et al., 2004). The submesoscale eddies are densely distribute over the entire SIO (Fig. 9d), which has a similar pattern to that of total eddies (Fig. 7a). The submesoscale anticyclonic eddies are densely distributed in the subtropical basin in central SIO. The area of high number of submesoscale anticyclonic eddies agrees well with location of the garbage patches, where drifters converge due to convergence of surface flow (Maximenko et al., 2012; Van Sebille et al., 2012).

3.3 Temporal variations

The occurrence of eddies shows significant seasonal variations (Fig. 10a), with more eddies in austral autumn and winter and less eddies in austral spring and summer. The number of cyclonic eddies reaches maximum in August, whereas the number of anticyclonic eddies reaches minimum in September. If the submesoscale eddies are not included, temporal variations of mesoscale eddies (Fig. 10b) are different from that of all eddies (Fig. 10a). The number of mesoscale eddies reach the maximum in October and the minimum in February, and the cyclonic and anticyclonic mesoscale eddies show similar seasonal variations.

To compare with seasonal variability of eddies detected from satellite observations, we use eddy data provided by Chelton et al. (2011). Because the number of drifter observations has increased dramatically since 1995 (Fig. 5a), we check eddy fields derived from altimetry SSH from 1995 to 2012. The result represents a similar temporal

distribution with Fig. 10b. There are more eddies generated in austral spring (Fig. 11), and less eddies in austral summer.

The vertical velocity shear associated with SICC and SEC system intensifies due to enhanced flux forcing of combined meridional Ekman and geostrophic convergence in austral spring (Jia et al., 2011). The seasonal change of baroclinic instability and EKE variations, induced by modulation of vertical velocity shear in the southeast Indian Ocean, favor the generation of eddies. In addition, other non-local processes including Leeuwin Current (Feng et al., 2007; Rennie et al., 2007) and Agulhas Current system (Backeberg et al., 2008; Beal et al., 2011) may also modulate the activity of mesoscale eddies. The mechanism of temporal variations of eddies needs further study.

4 Conclusions

Eddy characteristics in the SIO were investigated on the basis of in-situ satellite-tracked drifter data from 1979 to 2013. There are totally 19 252 eddies detected. Among them 7657 (11 595) are cyclonic (anticyclonic) eddies. For the submesoscale eddies, the ratio of cyclonic eddies (3183) to anticyclonic eddies (7182) is 1 to 2. Large eddies ($r \geq 100$ km) populate a band along 25° S, Mozambique Channel, and Agulhas Current. The populated region of large eddies has a large EKE (blue rectangle in Fig. 12). In the Mozambique Channel, the shape of large eddies is restrained by coastline in northeast-southwest direction.

The mesoscale eddy number shows significant seasonal variations, and are coherent with eddies generated in the SIO detected from altimetry observations. The spatial distribution of large eddies is overlapped with the large EKE region (Figs. 9a and 12). In the southeast Indian Ocean, vertical velocity shear results in seasonal baroclinic instability, and leads to seasonal EKE variations (Jia et al., 2011). Therefore, the mechanism of temporal distribution of eddies may be link to baroclinic instability. There are several main current systems in this region, including SICC-SEC, Leeuwin Current, and Agul-

Eddy characteristics in the SIO as inferred from surface drifter

Shaojun Zheng et al.

Title Page

Abstract

Introduction

Conclusions

References

Tables

Figures



Back

Close

Full Screen / Esc

Printer-friendly Version

Interactive Discussion



has Current system. The relationship between eddy activities and barotropic/baroclinic instabilities of currents should be studies in the future.

The dynamics of submesoscale eddies are distinct from the traditional mesoscale quasi-geostrophic theory (Thomas et al., 2008), and in situ submesoscale observation are still relatively scarce. Nencioli et al. (2013) estimated in situ submesoscale horizontal eddy diffusivity across an ocean front in the western Gulf of Lion in the Mediterranean Sea, which may extend our understanding about submesoscale process with more in-situ observations in the future.

Acknowledgements. We thank Wei Zhuang for useful discussions and comments. The satellite-tracked drifter data was provide by the Drifter Data Assembly Center (DAC) at NOAA's Atlantic Oceanographic and Meteorological Laboratory (<http://www.aoml.noaa.gov/envids/gld/index.php>). The drifter-derived mean flow data was also provided by DAC (http://www.aoml.noaa.gov/phod/dac/dac_meanvel.php). The mesoscale eddies data detected by altimeter observation were obtained from mesoscale eddies in altimeter observation of SSH (<http://cioss.coas.oregonstate.edu/eddies/>). The SLA data was provide by AVISO (<http://www.aviso.altimetry.fr/en/home.html>). This work was supported by "Strategic Priority Research Program" of the Chinese Academy of Sciences (XDA11010103), the Natural Science Foundation of China (41306018), the National Basic Research Program of China (2010CB950302, 2012CB955603), the Knowledge Innovation Program of the Chinese Academy of Sciences (SQ201108).

References

- Abraham, E. R.: The generation of plankton patchiness by turbulent stirring, *Nature*, 391, 577–580, doi:10.1038/35361, 1998.
- Abraham, E. R., Law, C. S., Boyd, P. W., Lavender, S. J., Maldonado, M. T., and Bowie, A. R.: Importance of stirring in the development of an iron-fertilized phytoplankton bloom, *Nature*, 407, 727–730, doi:10.1038/35037555, 2000.
- Aristegui, J., Tett, P., HernandezGuerra, A., Basterretxea, G., Montero, M. F., Wild, K., Sangra, P., HernandezLeon, S., Canton, M., GarciaBraun, J. A., Pacheco, M., and Barton, E. D.: The influence of island-generated eddies on chlorophyll distribution: a study of mesoscale

OSD

11, 2879–2905, 2014

Eddy characteristics in the SIO as inferred from surface drifter

Shaojun Zheng et al.

Title Page

Abstract

Introduction

Conclusions

References

Tables

Figures

⏪

⏩

◀

▶

Back

Close

Full Screen / Esc

Printer-friendly Version

Interactive Discussion



Eddy characteristics in the SIO as inferred from surface drifter

Shaojun Zheng et al.

Title Page

Abstract

Introduction

Conclusions

References

Tables

Figures



Back

Close

Full Screen / Esc

Printer-friendly Version

Interactive Discussion



variation around Gran Canaria, *Deep-Sea Res. Pt. I*, 44, 71–96, doi:10.1016/S0967-0637(96)00093-3, 1997.

Backeberg, B. C., Johonnesen, J. A., Bertino, L., and Reason, C. J.: The greater Agulhas Current system: an integrated study of its mesoscale variability, *Journal of Operational Oceanography*, 1, 29–44, 2008.

Beal, L. M., De Ruijter, W. P. M., Biastoch, A., Zahn, R., and SCOR/WCRP/IAPSO Working Group 136: On the role of the Agulhas system in ocean circulation and climate, *Nature*, 472, 429–436, doi:10.1038/Nature09983, 2011.

Berti, S., Dos Santos, F. A., Lacorata, G., and Vulpiani, A.: Lagrangian drifter dispersion in the southwestern Atlantic Ocean, *J. Phys. Oceanogr.*, 41, 1659–1672, doi:10.1175/2011jpo4541.1, 2011.

Chaigneau, A. and Pizarro, O.: Eddy characteristics in the eastern South Pacific, *J. Geophys. Res.-Oceans*, 110, C06005, doi:10.1029/2004jc002815, 2005.

Chelton, D. B., DeSzoeke, R. A., Schlax, M. G., El Naggar, K., and Siwertz, N.: Geographical variability of the first baroclinic Rossby radius of deformation, *J. Phys. Oceanogr.*, 28, 433–460, doi:10.1175/1520-0485(1998)028<0433:Gvotfb>2.0.Co;2, 1998.

Chelton, D. B., Schlax, M. G., and Samelson, R. M.: Global observations of nonlinear mesoscale eddies, *Prog. Oceanogr.*, 91, 167–216, doi:10.1016/j.pocean.2011.01.002, 2011.

Crawford, W. R., Brickley, P. J., Peterson, T. D., and Thomas, A. C.: Impact of Haida eddies on chlorophyll distribution in the Eastern Gulf of Alaska, *Deep-Sea Res. Pt. II*, 52, 975–989, doi:10.1016/j.dsr2.2005.02.011, 2005.

de Ruijter, W. P. M., Ridderinkhof, H., Lutjeharms, J. R. E., Schouten, M. W., and Veth, C.: Observations of the flow in the Mozambique Channel, *Geophys. Res. Lett.*, 29, 1502, doi:10.1029/2001gl013714, 2002.

de Ruijter, W. P. M., van Aken, H. M., Beier, E. J., Lutjeharms, J. R. E., Matano, R. P., and Schouten, M. W.: Eddies and dipoles around South Madagascar: formation, pathways and large-scale impact, *Deep-Sea Res. Pt. I*, 51, 383–400, doi:10.1016/j.dsr.2003.10.011, 2004.

Deverdiere, A. C.: Lagrangian eddy statistics from surface drifters in the eastern North-Atlantic, *J. Mar. Res.*, 41, 375–398, 1983.

Dong, C., McWilliams, J. C., Liu, Y., and Chen, D.: Global heat and salt transports by eddy movement, *Nature Communications*, 5, 3294, doi:10.1038/ncomms4294, 2014.

Dong, C. M., Liu, Y., Lumpkin, R., Lankhorst, M., Chen, D., McWilliams, J. C., and Guan, Y. P.: A scheme to identify loops from trajectories of oceanic surface drifters: an application in the

Eddy characteristics in the SIO as inferred from surface drifter

Shaojun Zheng et al.

Title Page

Abstract

Introduction

Conclusions

References

Tables

Figures



Back

Close

Full Screen / Esc

Printer-friendly Version

Interactive Discussion



Kuroshio extension region, *J. Atmos. Ocean. Tech.*, 28, 1167–1176, doi:10.1175/Jtech-D-10-05028.1, 2011.

Donners, J. and Drijfhout, S. S.: The Lagrangian view of South Atlantic Inter-ocean exchange in a global ocean model compared with inverse model results, *J. Phys. Oceanogr.*, 34, 1019–1035, doi:10.1175/1520-0485(2004)034<1019:Tlvosa>2.0.Co;2, 2004.

Falkowski, P. G., Ziemann, D., Kolber, Z., and Bienfang, P. K.: Role of Eddy pumping in enhancing primary production in the ocean, *Nature*, 352, 55–58, doi:10.1038/352055a0, 1991.

Feng, M., Majewski, L. J., Fandry, C. B., and Waite, A. M.: Characteristics of two counter-rotating eddies in the Leeuwin Current system off the Western Australian coast, *Deep-Sea Res. Pt. II*, 54, 961–980, doi:10.1016/j.dsr2.2006.11.022, 2007.

Gordon, A. L., Weiss, R. F., Smethie, W. M., and Warner, M. J.: Thermocline and intermediate water communication between the South-Atlantic and Indian Oceans, *J. Geophys. Res.-Oceans*, 97, 7223–7240, doi:10.1029/92jc00485, 1992.

Hamilton, P.: Eddy statistics from Lagrangian drifters and hydrography for the northern Gulf of Mexico slope, *J. Geophys. Res.-Oceans*, 112, C09002, doi:10.1029/2006jc003988, 2007.

Hansen, D. and Herman, A.: Temporal sampling requirements for surface drifting buoys in the tropical Pacific, *J. Atmos. Ocean. Tech.*, 6, 599–607, 1989.

Hansen, D. V. and Poulain, P. M.: Quality control and interpolations of WOCE-TOGA drifter data, *J. Atmos. Ocean. Tech.*, 13, 900–909, doi:10.1175/1520-0426(1996)013<0900:qcaiw>2.0.co;2, 1996.

Jia, F., Wu, L., and Qiu, B.: Seasonal Modulation of Eddy Kinetic Energy and Its Formation Mechanism in the southeast Indian Ocean, *J. Phys. Oceanogr.*, 41, 657–665, doi:10.1175/2010jpo4436.1, 2011.

Lankhorst, M.: A self-contained identification scheme for eddies in drifter and float trajectories, *J. Atmos. Ocean. Tech.*, 23, 1583–1592, doi:10.1175/Jtech1931.1, 2006.

Lankhorst, M. and Zenk, W.: Lagrangian observations of the middepth and deep velocity fields of the northeastern Atlantic Ocean, *J. Phys. Oceanogr.*, 36, 43–63, doi:10.1175/jpo2869.1, 2006.

Ledwell, J. R., Watson, A. J., and Law, C. S.: Evidence for Slow Mixing across the Pycnocline from an Open-Ocean Tracer-Release Experiment, *Nature*, 364, 701–703, doi:10.1038/364701a0, 1993.

Eddy characteristics in the SIO as inferred from surface drifter

Shaojun Zheng et al.

[Title Page](#)[Abstract](#)[Introduction](#)[Conclusions](#)[References](#)[Tables](#)[Figures](#)[Back](#)[Close](#)[Full Screen / Esc](#)[Printer-friendly Version](#)[Interactive Discussion](#)

Lévy M. and Klein, P.: Does the low frequency variability of mesoscale dynamics explain a part of the phytoplankton and zooplankton spectral variability?, *P. R. Soc. London*, 460, 1673–1683, 2004.

Lévy, M., Klein, P., and Tréguier, A. M.: Impacts of submesoscale physics on phytoplankton production and subduction, *J. Mar. Res.*, 59, 535–565, 2001.

Li, J., Zhang, R., and Jin, B.: Eddy characteristics in the northern South China Sea as inferred from Lagrangian drifter data, *Ocean Sci.*, 7, 661–669, doi:10.5194/os-7-661-2011, 2011.

Lumpkin, R. and Johnson, G. C.: Global ocean surface velocities from drifters: mean, variance, El Niño–Southern Oscillation response, and seasonal cycle, *J. Geophys. Res.-Oceans*, 118, 2992–3006, doi:10.1002/Jgrc.20210, 2013.

Lumpkin, R. and Pazos, M.: Measuring surface currents with Surface Velocity Program drifters: the instrument, its data, and some recent results, *Lagrangian analysis and prediction of coastal and ocean dynamics*, 39–67, 2007.

Maximenko, N., Hafner, J., and Niiler, P.: Pathways of marine debris derived from trajectories of Lagrangian drifters, *Mar. Pollut. Bull.*, 65, 51–62, doi:10.1016/j.marpolbul.2011.04.016, 2012.

McWilliams, J. C.: The nature and consequences of oceanic Eddies, in: *Ocean Modeling in an Eddying Regime*, edited by: Hecht, M. W. and Hasumi, H., American Geophysical Union, Washington D.C., 5–15, doi:10.1029/177GM03, 2013.

Morrow, R., Birol, F., Griffin, D., and Sudre, J.: Divergent pathways of cyclonic and anti-cyclonic ocean eddies, *Geophys. Res. Lett.*, 31, L24311, doi:10.1029/2004gl020974, 2004.

Nencioli, F., d'Ovidio, F., Doglioli, A. M., and Petrenko, A. A.: In situ estimates of submesoscale horizontal eddy diffusivity across an ocean front, *J. Geophys. Res.-Oceans*, 118, 7066–7080, doi:10.1002/2013jc009252, 2013.

Palastanga, V., van Leeuwen, P. J., and de Ruijter, W. P. M.: A link between low-frequency mesoscale eddy variability around Madagascar and the large-scale Indian Ocean variability, *J. Geophys. Res.-Oceans*, 111, C09029, doi:10.1029/2005jc003081, 2006.

Pujol, M. I. and Larnicol, G.: Mediterranean sea eddy kinetic energy variability from 11 years of altimetric data, *J. Marine Syst.*, 58, 121–142, doi:10.1016/j.jmarsys.2005.07.005, 2005.

Qiu, B. and Chen, S. M.: Eddy-induced heat transport in the subtropical North Pacific from Argo, TMI, and altimetry measurements, *J. Phys. Oceanogr.*, 35, 458–473, doi:10.1175/jpo2696.1, 2005.

Eddy characteristics in the SIO as inferred from surface drifter

Shaojun Zheng et al.

Title Page

Abstract

Introduction

Conclusions

References

Tables

Figures



Back

Close

Full Screen / Esc

Printer-friendly Version

Interactive Discussion



- Quartly, G. D. and Srokosz, M. A.: Eddies in the southern Mozambique Channel, *Deep-Sea Res. Pt. II*, 51, 69–83, doi:10.1016/j.dsr2.2003.03.001, 2004.
- Quartly, G. D., Buck, J. J. H., Srokosz, M. A., and Coward, A. C.: Eddies around Madagascar – the retroflexion re-considered, *J. Marine Syst.*, 63, 115–129, doi:10.1016/j.jmarsys.2006.06.001, 2006.
- Rennie, S. J., Pattiaratchi, C. P., and McCauley, R. D.: Eddy formation through the interaction between the Leeuwin Current, Leeuwin Undercurrent and topography, *Deep-Sea Res. Pt. II*, 54, 818–836, doi:10.1016/j.dsr2.2007.02.005, 2007.
- Ridderinkhof, H., van der Werf, P. M., Ullgren, J. E., van Aken, H. M., van Leeuwen, P. J., and de Ruijter, W. P. M.: Seasonal and interannual variability in the Mozambique Channel from moored current observations, *J. Geophys. Res.-Oceans*, 115, C06010, doi:10.1029/2009jc005619, 2010.
- Schott, F. A. and McCreary, J. P.: The monsoon circulation of the Indian Ocean, *Prog. Oceanogr.*, 51, 1–123, doi:10.1016/S0079-6611(01)00083-0, 2001.
- Schott, F. A., Xie, S. P., and McCreary, J. P.: Indian Ocean circulation and climate variability, *Rev. Geophys.*, 47, Rg1002, doi:10.1029/2007rg000245, 2009.
- Schouten, M. W., de Ruijter, W. P. M., van Leeuwen, P. J., and Ridderinkhof, H.: Eddies and variability in the Mozambique Channel, *Deep-Sea Res. Pt. II*, 50, 1987–2003, doi:10.1016/s0967-0645(03)00042-0, 2003.
- Schroeder, K., Chiggiato, J., Haza, A. C., Griffa, A., Ozgokmen, T. M., Zanasca, P., Molcard, A., Borghini, M., Poulain, P. M., Gerin, R., Zambianchi, E., Falco, P., and Trees, C.: Targeted Lagrangian sampling of submesoscale dispersion at a coastal frontal zone, *Geophys. Res. Lett.*, 39, L11608, doi:10.1029/2012gl051879, 2012.
- van Sebille, E., England, M. H., and Froyland, G.: Origin, dynamics and evolution of ocean garbage patches from observed surface drifters, *Environ. Res. Lett.*, 7, 044040, doi:10.1088/1748-9326/7/4/044040, 2012.
- Volkov, D. L., Lee, T., and Fu, L.-L.: Eddy-induced meridional heat transport in the ocean, *Geophys. Res. Lett.*, 35, L20601, doi:10.1029/2008gl035490, 2008.
- Zhang, Z. G., Wang, W., and Qiu, B.: Oceanic mass transport by mesoscale eddies, *Science*, 345, 322–324, doi:10.1126/science.1252418, 2014.
- Zu, T. T., Chen, J., and Wang, D. X.: Detection of the Cyclonic Eddy in the southwest of the South China Sea: from remote sensing data and drifter buoys, *Adv. Intel. Soft. Compu.*, 142, 153–159, 2012.

Eddy characteristics in the SIO as inferred from surface drifter

Shaojun Zheng et al.

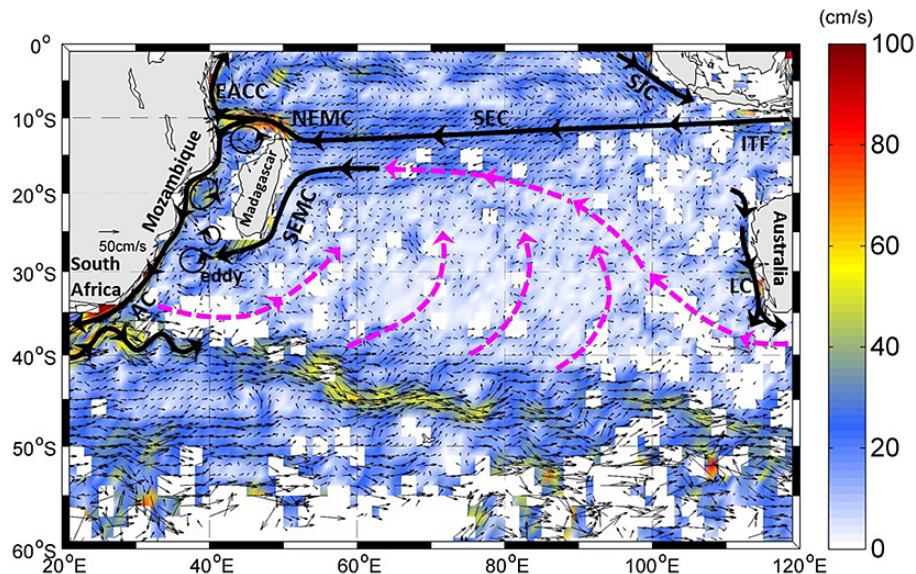


Figure 1. A Schematic diagram of identified current branches in the South Indian Ocean, modified from Schott et al. (2009) and Beal et al. (2011). Mean flow in the SIO is from the average of drifter-detected velocity in bins with $1^\circ \times 1^\circ$ resolution, and velocity less than 5 cm s^{-1} is omitted. (data details refer to Lumpkin and Johnson, 2013). Schematic current branches are the South Java Current (SJC), Indonesian Troughflow (ITF), South Equatorial Current (SEC), Northeast and Southeast Madagascar Current (NEMC and SEMC), East African Coast Current (EACC), AC (Agulhas Current), and Leeuwin Current (LC). The subsurface return flow is shown in magenta.

Title Page

Abstract

Introduction

Conclusions

References

Tables

Figures



Back

Close

Full Screen / Esc

Printer-friendly Version

Interactive Discussion



Eddy characteristics in the SIO as inferred from surface drifter

Shaojun Zheng et al.

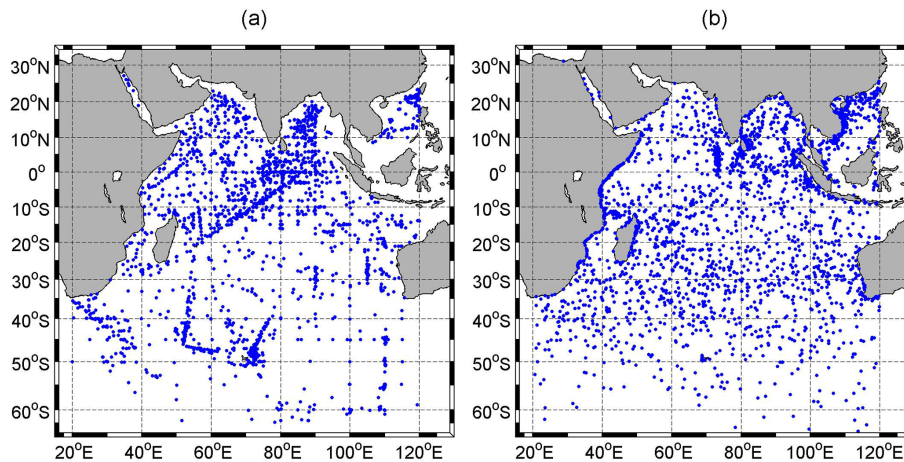


Figure 2. (a) Released and (b) terminated locations of surface drifter.

[Title Page](#)[Abstract](#)[Introduction](#)[Conclusions](#)[References](#)[Tables](#)[Figures](#)[Back](#)[Close](#)[Full Screen / Esc](#)[Printer-friendly Version](#)[Interactive Discussion](#)

Eddy characteristics in the SIO as inferred from surface drifter

Shaojun Zheng et al.

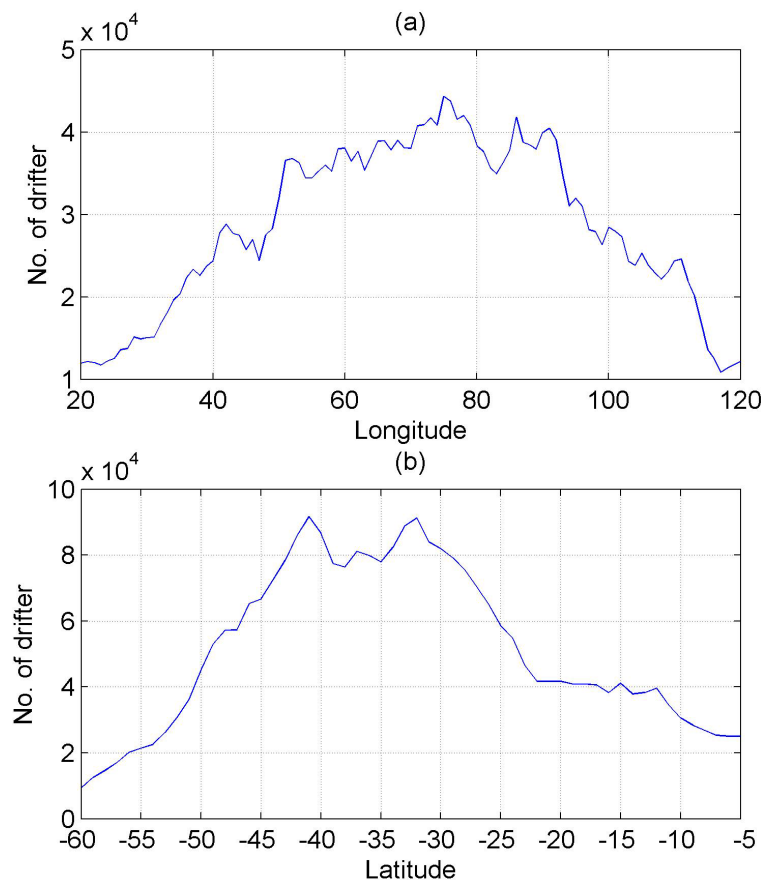


Figure 4. (a) Meridional and (b) zonal accumulated number of drifters as a function of longitude and latitude, respectively.

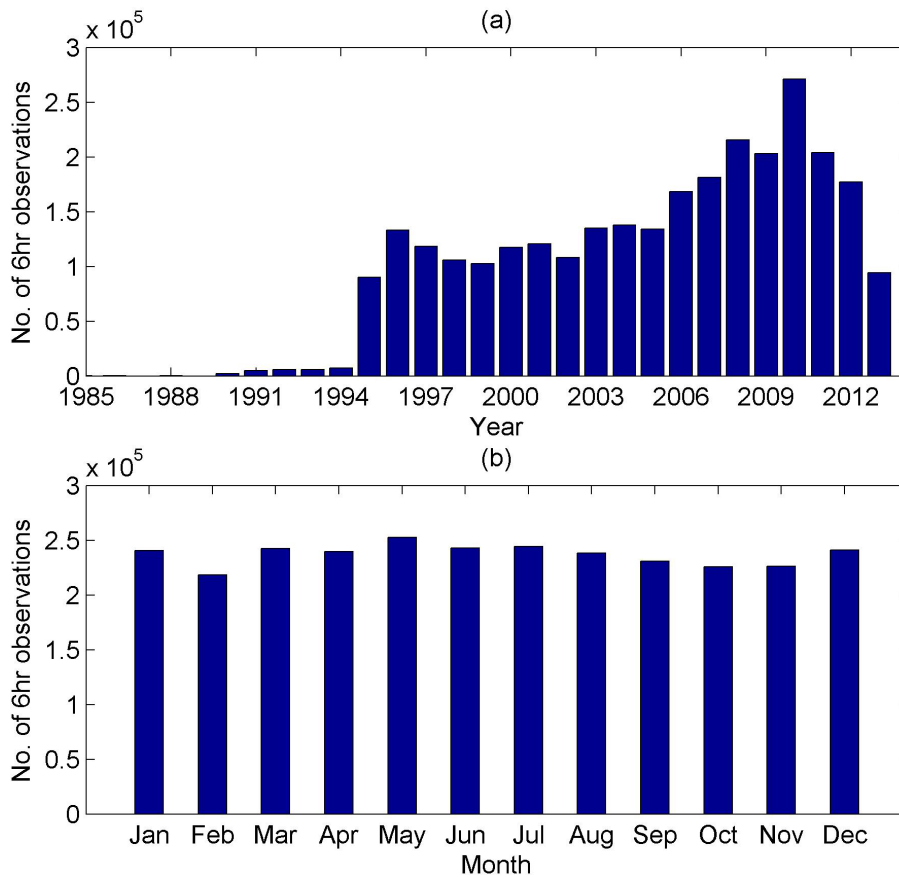


Figure 5. (a) Number of all drifter observations in each year since 1985, each observation is one six-hour position from a drifter trajectory. (b) Number of all drifter observations at six-hour intervals in each climatological calendar month.

Eddy characteristics in the SIO as inferred from surface drifter

Shaojun Zheng et al.

Title Page	
Abstract	Introduction
Conclusions	References
Tables	Figures
◀	▶
◀	▶
Back	Close
Full Screen / Esc	
Printer-friendly Version	
Interactive Discussion	



Eddy characteristics in the SIO as inferred from surface drifter

Shaojun Zheng et al.

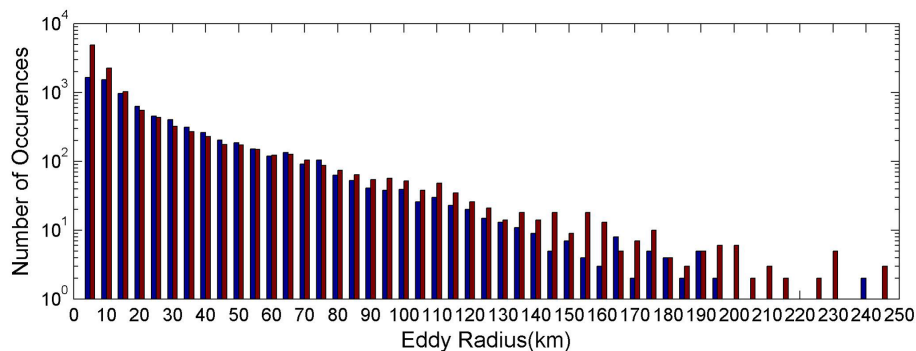


Figure 6. Histogram of eddy occurrence with bin width of 5 km for eddy radius. Blue and red bars indicates cyclonic and anticyclonic eddies, respectively.

[Title Page](#)[Abstract](#)[Introduction](#)[Conclusions](#)[References](#)[Tables](#)[Figures](#)[Back](#)[Close](#)[Full Screen / Esc](#)[Printer-friendly Version](#)[Interactive Discussion](#)

**Eddy characteristics
in the SIO as inferred
from surface drifter**

Shaojun Zheng et al.

Title Page

Abstract

Introduction

Conclusions

References

Tables

Figures



Back

Close

Full Screen / Esc

Printer-friendly Version

Interactive Discussion

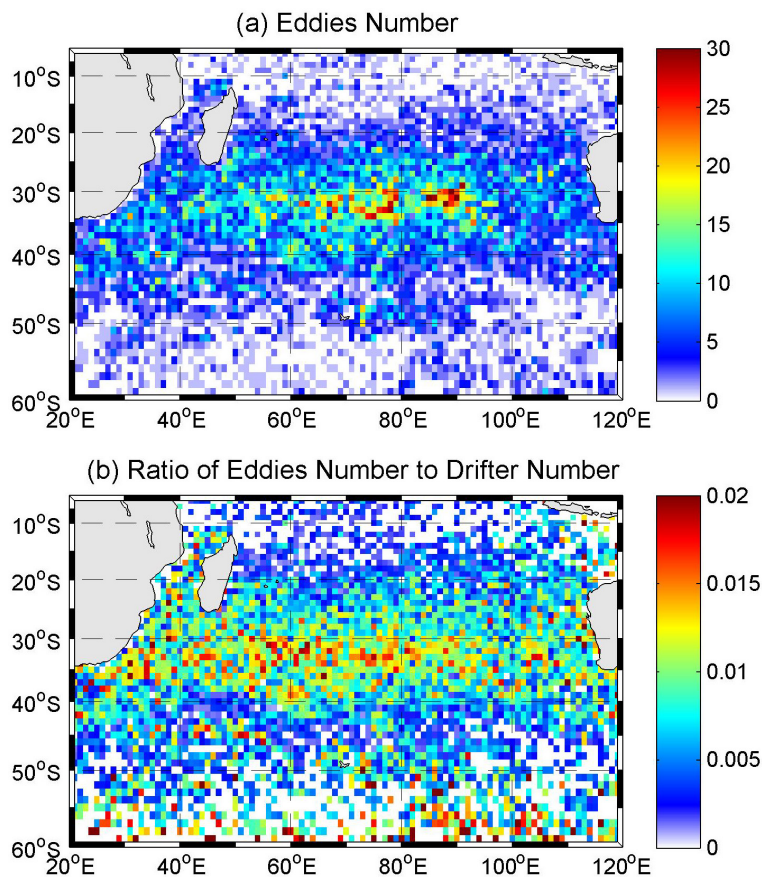


Figure 7. (a) Number of eddies detected in $1^\circ \times 1^\circ$ bin. (b) Ratio of eddies number to drifters number in $1^\circ \times 1^\circ$ bin.

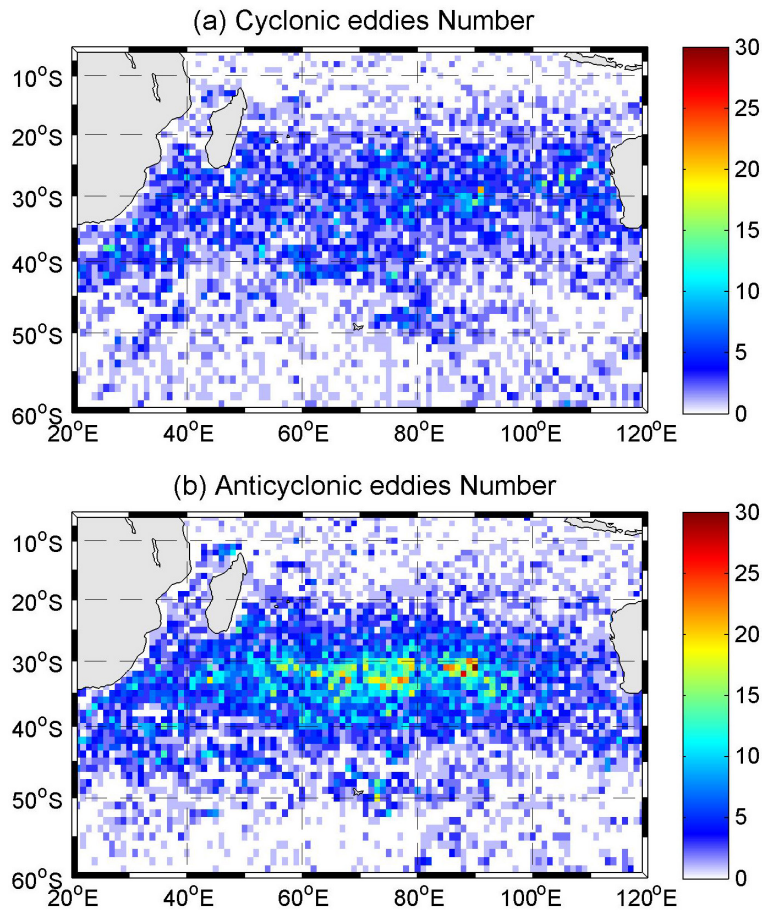


Figure 8. (a) Number of cyclonic eddies detected in $1^\circ \times 1^\circ$ bin. (b) Same as (a) but for anticyclonic eddies.

Eddy characteristics in the SIO as inferred from surface drifter

Shaojun Zheng et al.

Title Page

Abstract Introduction

Conclusions References

Tables Figures

◀ ▶

◀ ▶

Back Close

Full Screen / Esc

Printer-friendly Version

Interactive Discussion



Eddy characteristics in the SIO as inferred from surface drifter

Shaojun Zheng et al.

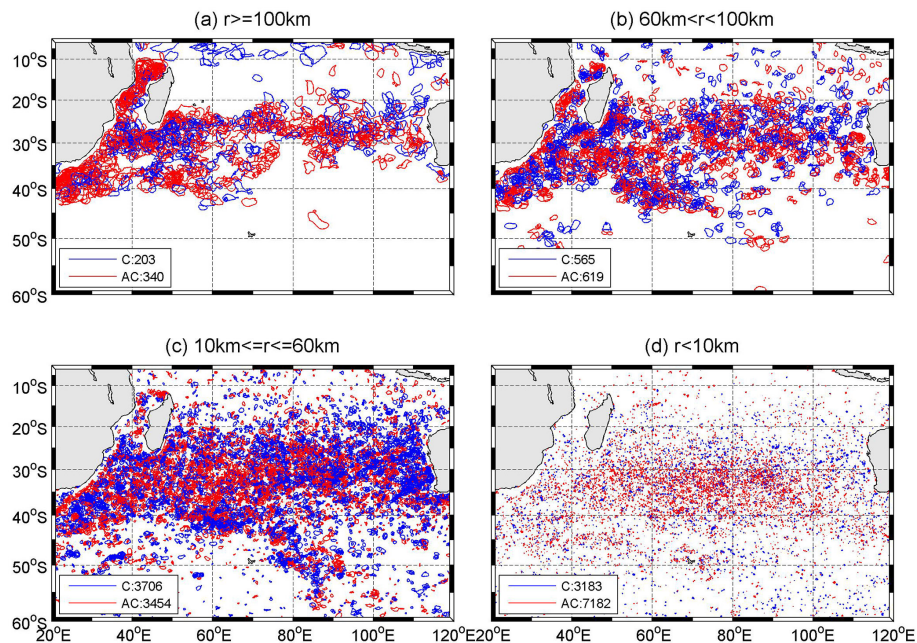


Figure 9. The distribution of cyclonic and anticyclonic eddies detected from drifters in the SIO.

Title Page

Abstract

Introduction

Conclusions

References

Tables

Figures



Back

Close

Full Screen / Esc

Printer-friendly Version

Interactive Discussion



